Evidence of inverse cascades in the cerebral dynamics: Spontaneous symmetry breaking during arterial inflow

Christian Kerskens and David López Pérez
Institute of Neuroscience, Trinity College, Dublin, Ireland

Cerebral fluid dynamics require a reverse energy mechanism to transport water and metabolites from tissue into veins [1–3]. Recent findings in active flow of bacteria have shown that such a mechanism involving backward energy cascades, so-called inverse cascades [4] may exist only during spontaneously broken mirror-symmetries [5–7]. Here, we wanted to investigate whether and, if so when symmetries break during a heart cycle. We used multiple spin echos (MSE)s [8–10] in magnetic resonance imaging (MRI) which can detect broken spherical symmetries. We found MSEs in brain tissue which appeared during arterial pulsation in a highly synchronized fashion in most parts of the brain. The timing suggests that the reverse energy flow is initiated during the energy injection of the heartbeat and ends with the isovolumetric vessel contraction. This interleaved process may explain how the illusive pulse wave traveling through the brain emerges as well as underlying principles of cerebral autoregulation and neurovascular coupling [3].

INTRODUCTION

During cerebral pulsation, water, that flows into the brain, decays via cascades guided by arteries, arterioles, capillaries to smaller scales. Eventually, this decay must reverse to find a way out towards the venous system [11]. What sounds simple is, in practice, a rare phenomena in 3D flow [6].

Only recently, such reverse energy flows, so-called inverse cascades, have been reported in floating bacteria during spontaneous mirror-symmetry breaking [12]. Brain cells may act in a similar way like bacteria although brain cells are not moving but instead the surrounding fluid. The key mechanism, the desired mirror symmetry breaking, causes spherical symmetry breaking in static brain cells which is accessible with magnetic resonance imaging (MRI) contrast.

In MRI, so-called multiple spin echos (MSEs) [13–15] or intermolecular multiple quantum coherences (iMQCs) [16, 17] result from broken spherical symmetries in the non-linear demagnetization field. The asymmetry can be introduced or amplified by gradient fields [13, 15, 16], RF pulses [18], and local field-inhomogeneities and anisotropies [19–22].

Two radio-frequency (RF) pulses combined with a magnetic field gradient are sufficient to generate MSEs with the consequence, that MSEs are present in many MRI sequences, especially in imaging series which are rapidly repeated. There, crusher gradients are added between two acquisitions with the primary intent to dephase any signal that remains from the previous excitation. This is where MSEs come into the game. They appear where the linear single spin echos (SSEs) disappear due to dephasing.

In an imaging series with fast repetitions, SSEs and MSEs reach a steady state which then, in case of a human brain, are disturbed by movement and physiological changes. Possible signal alternations which follow from the Bloch equations can be detected in both, SSEs and MSEs. These include changes of the magnetization vector $\vec{M}_0$ which can be changed by brain movement, flow, and to some extent by diffusion and changes in T_1, T_2 and ${T_2}^*$ relaxation. In contrast, symmetry changes which do not influence the Bloch equations directly are exclusive to MSEs.

In our experiments, we used a conventional single-slice gradient-echo echo planar imaging (GE-EPI) series with a short repetition time (TR) instead of a dedicated MSE sequence. While this had some limitations towards the variability of some sequence parameters, it allowed a simultaneous acquisition of SSE and MSE with the intent to isolate a MRI signal that was caused by broken symmetries.

RESULTS

With this sequence, we found predominate alternations with the cardiac frequency in brain tissue. In each cardiac cycle, we observed a period which varied in length between 150 and 420 ms showing an alternating signal of up to 15 % as plotted in Figure 1 and 2A to which we will refer in the following as zigzags.

The start of the period depended strongly on the head's mobility. The zigzags as shown in Figure 2A were achieved using additional cushions inside the coil and by breath-holding (without taking a deep breath). Zigzag lengthened in coherence with the breath-holding. It showed no delayed blood flow response to the PCO_2 challenge which we found in the blood vessels (not shown here). Under normal condition, the zigzags usually only contain two or three maxima as shown in Figure 2B during the first 10 s from 50 s to 60 s. At 60 s, the volunteer was instructed to hyperventilate with the result that the zigzags immediately disappeared.

We used an finger pulse oximeter and MRI data of the superior sagittal sinus to find reference time frames for

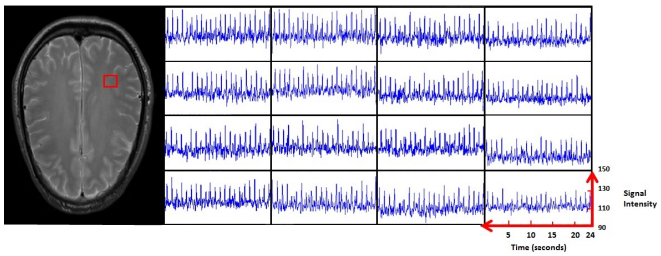

Figure 1. A 4x4 voxel matrix randomly picked. On the left, the red square shows location in the brain slice. On the right, 16 corresponding signal time courses of 24 s displaying the local tissue responses.

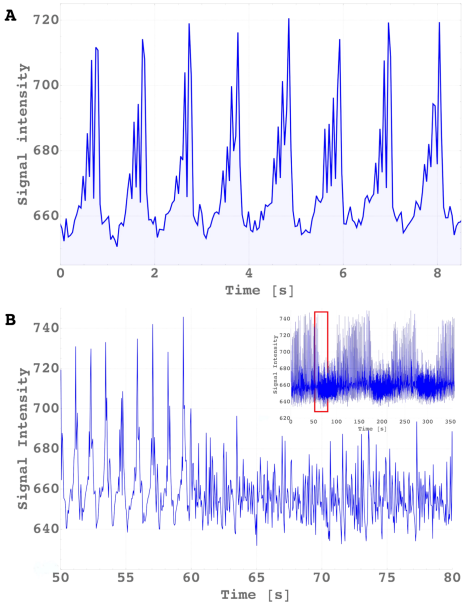

Figure 2. **A**: Whole-slice averaged signal time course (selected by a mask) during 8 heart cycles. Subject had extra head fixation and was instructed to breath-hold during the period. In contrast to signals in the veins (not shown here), zigzag signal showed no response to CO2 activity other than an immediate lengthening of the zigzag. **B**: Whole-slice averaged signal time course during normal breathing first. At 60 s, the subject was instructed to hyperventilate. The inlet shows the total time course with 3 hyperventilation periods and the selected time interval in red.

the zigzag pattern. We found that the zigzags always appeared during the arterial inflow phase. The abrupt end of the zigzags were coincident with the end-phase of the arterial pulse as shown in Figure 3A and the rise of venous outflow as demonstrated in Figure 3B.

We located the zigzags in tissue over the entire brain tissue except in areas which are known to be prone to motion like the periventricular area [23] as shown in Figure 4. Regions like skull, ventricle etc and in the attached test tubes showed no zigzags. Otherwise, we found that

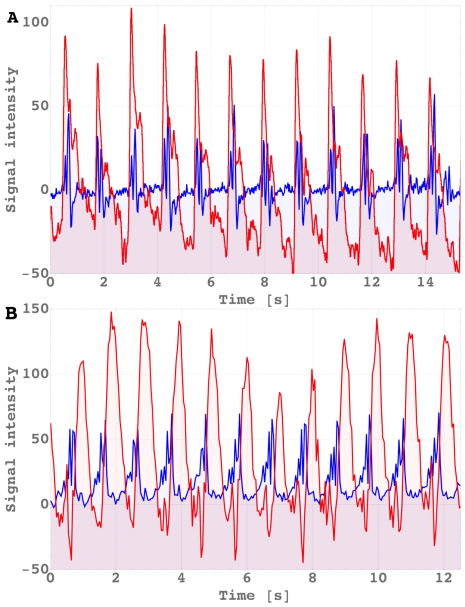

Figure 3. Signal time course (Blue) during 12 heart cycles compared with **A**: Simultaneous oximeter reading of a finger (Red) and **B**: Signal time course (Red) of a vein.

the zigzag, including the sudden end, could be restored while being averaged over the whole imaging slice Figure 2A.

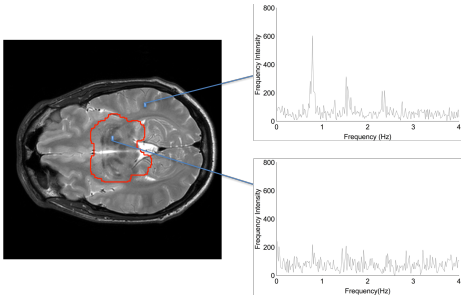

Figure 4. Fourier-Transform of two representative voxel. Surrounded tissue (red drawing) on the left shows signal dependency as shown in the bottom plot.

For investigation of the underlying contrast mechanism, we varied the following sequence parameters using the averaged signal: (a) the slice angulation, (b) the off-resonance frequency of the saturation pulses, (c) the flip angle (FA) with saturation pulses, and (d) the flip angle (FA) without saturation pulses.
For (a), we found the angle dependency of the demagnetization field as shown in Figure 5A where φ is the angle between the slice gradient and the main magnet field. The plot represents the fitted function $|(3 \cdot cos^2[\varphi_{cor}]-1)|$ where φ_{cor} takes additional gradients in read direction into account. Adjusted R^2 test of goodness-of-fit resulted in R^2=0.9958.

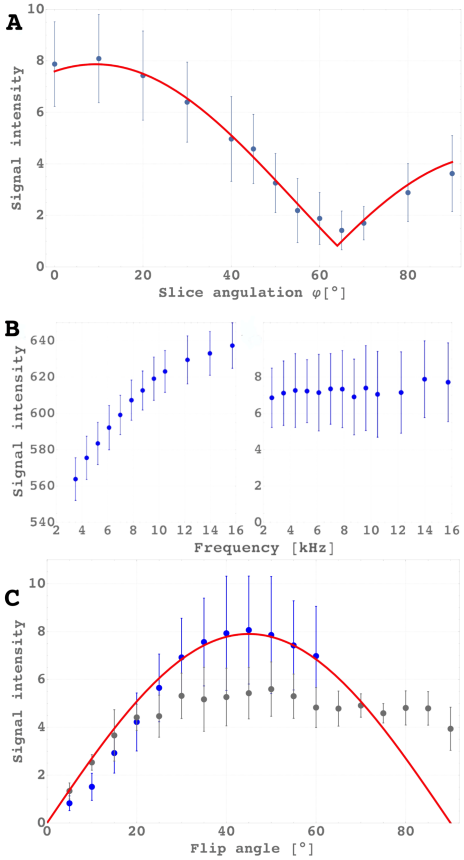

Figure 5. Variation of sequence parameters. Data shows signal averaged over 5 subjects. Error bars represent the standard deviation from the mean. **A**: Signal intensity plotted against the slice gradient angulation φ in respect to the magnetic main field. **B**: Signal intensity plotted against the frequency offset of the saturation slices of the averaged baseline signal (left) and averaged signal of cardiac pattern (right). **C**: Whole-slice averaged signal time course plotted against flip angle variation with saturation pulses (Blue) and without (Grey). IZQC prediction plotted in Red.

For (b), we found a typical magnetization transfer contrast (MTC) change for the baseline signal which depended on the off-resonance frequency (Figure 5B, left-hand side). In contrast, the zigzag intensity showed no significant changes in the same frequency range (Figure 5B, right-hand side).
For (c), we found a maximum peak intensity at 45 ∘ (Figure 5C). It followed the predicted signal course for intermolecular Zero Quantum Coherence (iZQC) [24] in a range from 20 ∘ to 60∘ (R_2=0.9964).
For (d), we could extend our observation to 90 ∘ where we found a flat plateau following an initial signal increase. In comparison, with (c) the signal was lower from 25 ∘ onward as shown in Figure 5C.

DISCUSSION

We found alternating signals (zigzags) which showed, when the saturation pulses were applied, the remarkable immunity of iZQC to MTC [25] and the specific flip angle dependency of iZQC with a maximum at 45∘ [24]. Without the saturation pulses, we found a mixture of quantum orders which explains the destructive coherences (signal plateau from 30 ∘ onward) [26] dephasing the signal at higher flip angle.
The angle dependency in Figure 5A verified the MSE origin of the signal. From neglectable signal intensity at the magic angle, we could exclude SSEs as signal contrast. The missing SSE components rule out that the signal was generated by flow or movement, relaxation (including T^*_2-variation by blood oxygenation changes), field inhomogeneities or other multiple RF effects like stimulated echos.
Nevertheless, we investigated further if either flow or movement, the most reasonable signal sources due to the pulsative character, may have generated the signals. We could exclude movement because on the one hand increased movement destroyed the zigzag as demonstrated in the hyperventilation challenge, while on the other hand breath-holding, which reduced body movement, resulted in an immediate lengthening of the signal response. From the same experiment, we could exclude flow dependency because the zigzag did not respond to the CO_2 challenge, despite the fact, that we observed increased blood flow in major blood vessels (data not shown here). In a fMRI study [27], we could confirm further that local blood flow changes during visual activation left the MSEs undisturbed.
Finally, we can underpin the above arguments by the spatial and temporal distribution.The remarkable high synchronization of symmetry breaking over the entire brain, which is reflected by the fact that the zigzag is recoverable in the averaged signal time courses, demonstrates that effective circulation is a global matter. As such, it is unlikely that a global sudden change (the spontaneous symmetry breaking evolves extremely fast in just few milliseconds) can be overlooked with SSE or other non-MRI methods, if detectable. To our knowledge, similar observations have not been made yet which single out symmetry breaking as contrast mechanism.
In respect of brain dynamics, the timing of the zigzags during the arterial pulsation is consistent with the concept of the illusive brain wave [3] where the key mechanism of the reverse energy flow, the spontaneous mirror-symmetry breaking, falls together with the arterial pulse. Interestingly, we found that the zigzags decline in healthy aging and disappears completely with cognitive impairment [28].

METHODS

40 subjects (between 18 and 46 years old) were scanned in a 3.0 T Philips whole-body MRI scanner (Philips, The Netherlands) operated with a 32-channel array receiver coil. Imaging protocols using standard single-shot GE EPI sequence were approved by the Trinity College School of Medicine Research Ethics Committee.
In our consecutive EPI time series, only even-numbered readouts contained MSEs (whereby counting begins one readout before the broken symmetry occurs). The asymmetric gradient field (Figure 6), which are before the even-numbered slice-selection RF-pulses, generated then zero quantum orders [29].
Initial experiments were carried out to establish a protocol that could deliver stable cardiac related signals over a range of subjects. Initially, test tubes with a water solution (1000 ml demineralized water contained 770 mg $CuSO_45H_2O$, 1 ml Arquad (AkzoNobel), 0.15 ml H_2SO_4-(0.1 N)) were positioned close to the head for reference signals. The finalized parameters of the GE-EPI sequence were as follows: FA = 45°, TR = 45 ms and the TE = 5 ms with a voxel size was 3.5 x 3.5 x 3.5 mm, matrix size was 64x64, SENSE factor 3, bandwidth readout direction was 2148 Hz.

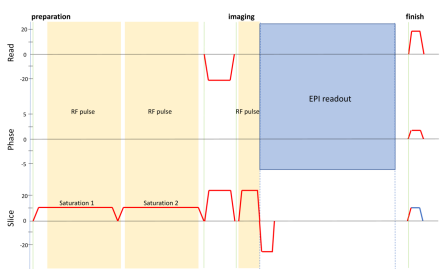

Figure 6. Gradient scheme of the EPI sequence with two saturation pulse.

Figure 6 shows the gradient scheme. Saturation gradients had a time integral (length x strength) of $\mathrm{Gt}_{sat} = 5.1$ ms x 6.25 mT/m, the crusher gradients in read and slice direction of $\mathrm{Gt}_{cru} = 1.3$ ms x 25 mT/m, the slice rephase gradient of $\mathrm{Gt}_{sr} = 0.65$ ms x 25 mT/m, the slice termination gradient of $\mathrm{Gt}_{st} = 0.65$ ms x 15 mT/m, and the total read dephase after EPI readout gradient of $\mathrm{Gt}_{rt} = 0.65$ ms x 22.5 mT/m. The angle between magnet field and gradient field was then

$$\varphi_{cor} = \varphi - \tan^{-1}\left[\frac{\mathrm{Gt}_{cru} - \mathrm{Gt}_{rt}}{2\mathrm{Gt}_{sat} + \mathrm{Gt}_{cru} + \mathrm{Gt}_{st}}\right] = \varphi - 9.6^\circ$$

where φ is the slice angulation. The imaging slice was set coronal above the ventricle. In addition, two saturation slices of 5 mm (15mm above and 20mm below) in thickness were placed parallel to the imaged slice. The following alternation (each with 1000 repetitions in five participants) were carried out, (a) slice angulation starting from coronal 0° to axial 90°in the steps as [0, 10, 20, 30, 40, 45, 50, 55, 60, 65, 70, 80, 90], (b) the distance of the REST slabs were varied between 0.8 mm and 50 mm to alter the off-resonance frequency. The off-resonance frequencies were [2.62, 3.49, 4.36, 5.23, 6.11, 6.98, 7.84, 8.73, 9.60, 10.47, 12.22, 13.96, 15.71, 17.45] kHz, (c) Flip angle was varied for the case with saturation pulses from 5° to 60° in steps of 5°(60°was the power limit by the specific absorption rate (SAR)) and without saturation pulses from 5°to 90° in steps of 5°, (d) 9 slices were acquired at different positions, with each slice matching from bottom to the top the position of those acquired in the anatomical scan. In four participants, we examined the motion sensitivity where we immobilized the head with multiple cushions. During indicated intervals the subjects were asked to stop breathing for 20 s or to hyperventilate for 40 s. Finally, anatomical MRI images in all studies included a high-resolution sagittal, T1-weighted MP-RAGE (TR = 2.1 s, TE = 3.93 ms, flip angle = 7).
Data were processed with Matlab 2014a (http://www.mathworks.co.uk/). Rescaling was applied to all data sets before any analysis using the MR vendor's instructions. Average time series were visually inspected in search for irregularities which were manually removed from the analysis leaving the rest of the time series unaltered. Manual segmentation was used to create a mask to remove cerebral spinal fluid (CSF) contributions. The first 100 scans were removed to avoid signal saturation effects. The manual segmentation of the masks was eroded to avoid partial volume effects at the edges. The cardiac signal and baseline detection was based on the method proposed in Gomes and Pereira [30]. Final data presentation was carried with Mathematica (Wolfram Research, Champaign, Illinois).

AUTHORS' CONTRIBUTIONS

D.L.P. and C.K. performed initial experiments, D.L.P. performed validation experiments and analyzed the data, C.K. designed the research and wrote the paper.

ACKNOWLEDGMENTS

We would like to thank S. Joseph for carrying out the imaging protocols for our participants, R. Fallon for reading the manuscript, and Science Foundation Ireland for supporting D.L.P. from 2011-2015 (SFI-11/RFP.1/NES/3051).

[1] S. B. Hladky and M. A. Barrand, Fluids and Barriers of the CNS **11**, 26 (2014).
[2] M. Nedergaard, Science **340**, 1529 (2013).
[3] C. Kerskens, "The illusive brain wave," (2018).
[4] R. H. Kraichnan, Journal of Fluid Mechanics **59**, 745 (1973).
[5] H. K. Moffatt, Journal of Fluid Mechanics **35**, 117–129 (1969).
[6] L. Biferale, S. Musacchio, and F. Toschi, Phys. Rev. Lett. **108**, 164501 (2012).
[7] J. Slomka and J. Dunkel, Proceedings of the National Academy of Sciences (2017).
[8] G. Deville, M. Bernier, and J. M. Delrieux, Physical Review B (1979).
[9] G. Eska, H. G. Willers, B. Amend, and C. Wiedemann, Physica B+ C (1981).
[10] R. Bowtell, R. M. Bowley, and P. Glover, Journal of Magnetic Resonance (1969) **88**, 643 (1990).
[11] C. Kerskens, "The illusive brain wave," (2018).
[12] J. Slomka and J. Dunkel, Proceedings of the National Academy of Sciences (2017).
[13] G. Deville, M. Bernier, and J. M. Delrieux, Physical Review B (1979).
[14] G. Eska, H. G. Willers, B. Amend, and C. Wiedemann, Physica B+ C (1981).
[15] R. Bowtell, R. M. Bowley, and P. Glover, Journal of Magnetic Resonance (1969) **88**, 643 (1990).
[16] W. S. Warren, W. Richter, A. H. Andreotti, and B. T. Farmer, Science **262**, 2005 (1993).
[17] E. D. Minot, P. T. Callaghan, and N. Kaplan, Journal of Magnetic Resonance **140**, 200 (1999).
[18] A. Jerschow, Chemical Physics Letters **296**, 466 (1998).
[19] L. S. Bouchard, R. Rizi, and W. Warren, Magn Reson Med **48**, 973 (2002).
[20] R. Bowtell, S. Gutteridge, and C. Ramanathan, Journal of Magnetic Resonance **150**, 147 (2001).
[21] S. Capuani, M. Alesiani, R. T. Branca, and B. Maraviglia, Solid State Nuclear Magnetic Resonance **25**, 153 (2004).
[22] L. S. Bouchard, F. W. Wehrli, C. L. Chin, and S. W. Warren, Journal of Magnetic Resonance **176**, 27 (2005).
[23] R. Nunes, P. Jezzard, and S. Clare, J Magn Reson **177**, 102 (2005).
[24] C. Zhong, Z. Shaokuan, and Z. Jianhui, Chemical Physics Letters **347**, 143 (2001).
[25] E. Uzi and N. Gil, Journal of Magnetic Resonance **190**, 149 (2008).
[26] J. Baum, M. Munowitz, A. N. Garroway, and A. Pines, Multiple-quantum dynamics in solid state NMR,J. Chem. Phys. 83, 2015 (1985) (1985).
[27] D. López-Pérez, *Non-Single Quantum MRI: A Cardiac Modulated Rhythm in the Brain Tissue*, Ph.D. thesis, Medicine (2016).
[28] D. López-Pérez, A. Bokde, and C. Kerskens, in preparation (2018).
[29] W. S. Warren, S. Ahn, M. Mescher, M. Garwood, K. Ugurbil, W. Richter, R. R. Rizi, J. Hopkins, and J. S. Leigh, Science **281**, 247 (1998).
[30] E. F. Gomes, A. M. Jorge, and P. J. Azevedo, in *Proceedings of the International C* Conference on Computer Science and Software Engineering* (ACM, 2013) pp. 23–30.